Metal ammonia solutions: A lattice model approach

Kevin Leung[a] and Félix S. Csajka[b]
Department of Chemistry, University of California at Berkeley, Berkeley, California 94720

(Received 1 December 1997; accepted 24 February 1998)

A generalized Falicov–Kimball model is applied to study the phase diagram of metal ammonia solutions. The model includes a fluid–fluid interaction term and an electron–fluid interaction with a hard core and an attractive tail. Mean-field theories are derived for the localized and delocalized electron phases using ideas from the slave-boson approach to the Hubbard model. The attractive force stabilizes both the homogeneous delocalized electron phase and a regime where the electrons localize in cavities devoid of fluid particles. In its absence, the localized states are found to be unstable towards phase separation, in contrast to previous predictions. The Gaussian fluctuations and structure factors derived from this theory suggest the existence of bicontinuous channels percolating through the system. These findings agree qualitatively with experiments and computer simulations. © *1998 American Institute of Physics.* [S0021-9606(98)50821-5]

I. INTRODUCTION

Group I and II metals spontaneously ionize in liquid ammonia and release their valence electrons, forming metal ammonia solutions. There is considerable interest in the properties of metal ammonia solutions,[1–6] which exhibit a variety of structural phases as well as a wide spectrum of electric and magnetic behaviors. At low temperature, the system segregates into metal-rich and metal-poor phases.[7] At low metal concentration, the excess electrons are solvated in cavities surrounded by ammonia molecules.[1,8] They absorb light in the visible range, which gives the solution its characteristic blue color. These localized electrons diffuse with their solvent cage and contribute minimally to electrical conductivity. As the metal concentration increases, the electrical conductivity experiences a sharp jump of several orders of magnitude within a small concentration range.[1,6] The structure of metal ammonia solutions has been investigated by Deng, Martyna, and Klein[9] using computer simulation. They find that well-localized electron-containing voids give way to percolating channels that support extended electronic states as the metal concentration increases. The crossover occurs at metal concentrations which are consistent with experimental data for the metal–insulator transition. This strongly suggests that structural changes accompany the metal–insulator transition (see Fig. 1).

The interplay between structural changes in the fluid and the quantum behavior of electrons, the effect of liquidlike disorder on electronic structure, and the competition between localized and extended electronic states makes this an interesting problem.[10,11] The simple lattice model proposed in this paper is designed to capture these features and reproduce the various phases of the system. The model is based on the Falicov–Kimball Hamiltonian which describes a many-fermion (electron) system coupled to classical lattice gas (fluid) degrees of freedom. The fermions are allowed to hop to their nearest-neighbor sites, but they are excluded from any site occupied by a lattice gas particle. An attractive tail is also included to model the electrostatic interaction between lattice gas and fermions, and a lattice gas–lattice gas attractive interaction.

The Kimball–Falicov Hamiltonian has been extensively studied, for example, in the context of metal–insulator transitions and as an approximation to the Hubbard model.[12–18] With only the on-site U interaction, the existence of lattice gas–fermion phase separation is well established (see, e.g., Ref. 18). The exact solution can be found in infinite dimensions,[14,16] and results obtained in that limiting case are considered useful ''mean-field'' descriptions in finite dimensions. However, self-averaging effects preclude localization in infinite dimensions. Furthermore, a systematic expansion in $1/d$, where d is the physical dimensionality, is somewhat problematic at large U.[19] Other methods of solution include the Hartree approximation[12] and the coherent potential approximation.[13] The former fails completely at large U. The latter treats quenched distributions of lattice gas as opposed to lattice gas annealed to electronic configurations. In addition, it does not guarantee a bound to the free energy.

In this paper, two separate mean-field theories are applied to treat fermions localized in cavities and delocalized fermions that percolate through the system, respectively. Localized and delocalized states are treated separately because approaching one from the other is nonperturbative and nontrivial.[20,21] The metal–insulator transition is identified as the phase boundary between the two phases. The theory for the localized fermion phase involves enumerating states in a finite sized cell or ''cavity.'' By allowing for the fact that such cavities can have multiple fermion occupancy, it is found that an attractive interaction between fermions and lattice gas molecules is essential for stabilizing the localized

[a]Author to whom all correspondence should be addressed; present address: Sandia National Laboratories, MS 1421, Albuquerque, New Mexico 87185. Electronic mail: kleung@sandia.gov
[b]Present address: Max-Planck Institute for Colloids and Interfaces, Kantstrasse 55, 14513 Teltow-Berlin, Germany.

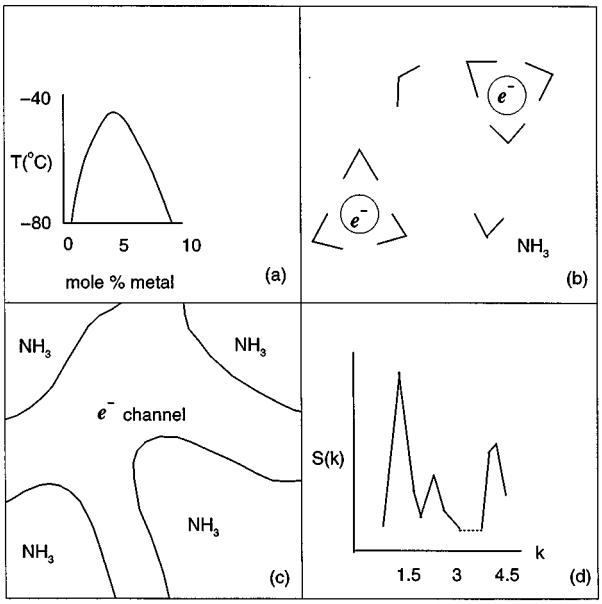

FIG. 1. Illustration of excess electrons in ammonia. (a) A caricature of the phase coexistence curve of sodium ammonia solutions (after Ref. 7); (b) low metal concentration: excess electrons (''e^-'') reside in cavities surrounded by ammonia molecules; (c) percolating channels that support extended electronic states appear at moderate to high metal concentrations (Ref. 9). The regions marked ''NH_3'' are occupied by ammonia molecules and counter ions; (d) illustration of the total structure factor computed in simulation studies (after Ref. 9) at moderate to high metal concentration. The dimensionless wave vector k is scaled by 3.6 Å, the Lennard-Jones diameter of ammonia molecules used in the simulation. The structure at $k\sim 2\pi$ describes ammonia–ammonia correlations, while the peak at $k\sim 1.5$ characterizes the bicontinuous structures.

phase with respect to phase separation, in contrast to previous predictions.[22] The extended phase treatment borrows from the slave-boson theory[23,24] often applied to Hubbard models. In these theories, auxiliary degrees of freedom are introduced to give reasonable approximations. They are particularly useful at large U, where conventional Hartree–Fock theories fail, and successfully describe the band narrowing or mass renormalization in Hubbard models. Band narrowing also occurs in the Kimball–Falicov model, which suggests that slave-boson-like treatments should be fruitful. It will be shown that, with a proper choice of auxiliary degrees of freedom, a lower bound to the free energy can be obtained for the strong-coupling Kimball–Falicov model, and the exactly known zero-hopping limit is also reproduced.

Fluctuations from mean-field behavior will be considered to Gaussian order. The correlation functions derived at this level of approximation are consistent with the bicontinuity observed in computer simulations.[9] These structures arise from the competing forces. The situation is reminiscent of oil–water–surfactant mixtures, which also exhibit bicontinuous, percolating ''microemulsion'' phases.[25,26] The physics of the two systems is actually closely related.[9,27] The surfactant molecules prevent the oil–water phase separation and give rise to various mesophases. Likewise, the bicontinuous and the cavity phases in metal ammonia solutions are stable because the electrostatic forces forces prevent the electron–ammonia phase separation. Electrons and ammonia molecules exclude each other due to the Pauli exclusion principle. If this were the only interaction, the two species would simply phase separate. Other systems with related physics are liquid metals and molten salts, which also exhibit metal–insulator transitions.[28]

The proposed model leaves out the Coulombic forces between the negatively charged electrons as well as their interaction with the metal counter ions. Simulation studies indicate that the metal ions can be replaced by a uniform charge background in the cavity-dominated regime, and they do not qualitatively affect the electronic states in general.[9] Similarly, the screened Coulomb interaction between the well-separated cavity electrons should only lead to minor large-length-scale effects.[29] Indeed, cavity formation seems to be driven by the large ($\sim$1 eV) solvation free energy for isolated electrons in polar solvents.[8,30] Even at high metal concentration, where extended electronic states dominate, the charge–charge interactions should be inhibited by the large ($\sim$20) dielectric constant of liquid ammonia. It is our assumption that the electron–electron repulsion is a secondary effect, and that the strong ammonia–electron interaction dominates even for the extended fermion phase. Neglecting the electron–electron interaction means that magnetic effects are unaccounted for[6,31,32] and some quantitative trends will be inaccurate. Notwithstanding its simplicity, it will be shown that the present lattice model exhibits many features found in metal ammonia solutions.[33]

Section II of this paper describes the model and the mean-field methods of solution. Fluctuations and correlation functions are derived in Sec. III. Section IV contains the results and Sec. V concludes this work with a discussion of the successes and shortcomings of the present model. A brief version of this work has been published in Ref. 34.

II. MODEL AND MEAN-FIELD METHOD OF SOLUTION

A. Hamiltonian

Consider the Kimball–Falicov Hamiltonian augmented with long-ranged attractive interactions,

$$H=\lim_{U\to\infty} -t\sum_{\langle ij\rangle\sigma} c_{i\sigma}^{+}c_{j\sigma}-\mu_e\sum_{i\sigma} c_{i\sigma}^{+}c_{i\sigma}-\mu_b\sum_i n_i + U\sum_{i\sigma} c_{i\sigma}^{+}c_{i\sigma}n_i-\sum_{i\neq j,\sigma} v_{ij}c_{i\sigma}^{+}c_{i\sigma}n_j -(1/2)\sum_{ij} w_{ij}n_in_j, \tag{1}$$

where $c_{i\sigma}^{+}$ ($c_{i\sigma}$) are fermionic creation (annihilation) operators of spin σ at site i, $U\to\infty$ is the on-site coupling between lattice gas and fermions, $v_{ij}>0$ is the off-site attraction between lattice gas and fermions, $w_{ij}>0$ is an attraction between lattice gas particles, μ_e and μ_b are the chemical potentials of the fermions and lattice gas, respectively, and $n_i=0,1$ describes the lattice gas degrees of freedom. In the strong coupling limit, the lattice gas and fermions cannot occupy the same site; hence the lattice gas particles, which exclude the fermions, will also be refered to as ''blockers.'' The thermodynamics of this model is computed to mean-field order at constant pressure and chemical composition.

B. Model for cavity phase

Fermions are assumed to localize in rectangular cylindrical cells or cavities of uniform shape $a_x \times a_y \times a_z$. There is no quantal hopping into or out of each cavity, and the cavity packing fraction is assumed to be small enough that the cells are independent. Each cell contains either fermions or blockers or is empty. Under these assumptions, the system is a superlattice, and the partition function factors. The mean-field Helmholtz energy per site is given by

$$\begin{aligned} -\beta f &= V_a^{-1} \log Z_{\text{cell}} \\ &= V_a^{-1} \log\{\Pi_{k\sigma}[1+e^{-\beta(E_k-\mu_e')}]+(1+e^{\beta\mu_b'})^{V_a} \\ &\quad -1\}-2\beta\bar{v}_0\rho_e\rho_b-(1/2)\beta\bar{w}_0\rho_b^2, \end{aligned} \tag{2}$$

where k indexes the particle-in-a-box states with energies E_k,

$$\bar{w}_0=\sum_j w_{ij}, \quad \bar{v}_0=\sum_j{}' \langle v_{ij}\rangle_i, \tag{3}$$

where i and j are restricted to different cells in the second (primed) summation, and the average is over all sites of a given cell. ρ_b and ρ_e are the blocker and single-spin fermion densities. They obtain from taking partial derivatives with respect to the chemical potentials. Finally, $\mu_b'=\mu_b+2\bar{v}_0\rho_e+\bar{w}_0\rho_b$, and $\mu_e'=\mu_e+\bar{v}_0\rho_b$. In summary, in Z_{cell} the lattice gas part is treated exactly, and the fermion part is assumed to factor into superlattice cells, with the off-site interaction treated to mean-field order.

When $v_{ij}=w_{ij}=0$ and $a_x=a_y=a_z=1$, there is no hopping, and the ''fermions'' are classical lattice gas particles that occupy one lattice site. Only one type of lattice gas is allowed per site, and Eq. (2) is exact in this limit. For finite v_{ij} and/or w_{ij}, the model is an asymmetric three-state Potts model with long-ranged interactions, and Eq. (2) obtains from a Gibbs–Bogoliubov–Feynman variational principle using a noninteracting Potts Hamiltonian as the reference. For $a_x, a_y, a_z > 1$, Eq. (2) describes a quantum extension of such a mean-field theory. (For simplicity, the spatial variation of electronic density has been neglected when estimating the fermion–blocker attraction between neighboring cells.) μ_e and μ_b are varied to give the desired pressure and chemical composition.

In the classical $t \to 0$ limit, $V_a=1$ lattice site is optimal, and the localized and extended fermion theories are identical. When two-phase coexistence is stable, $V_a \to \infty$, and the localized and extended fermion phase free energies agree with each other. Hence the two theories agree in the high and low temperature limits.

An important issue in localization is the role of the *mobility edge* or V_0. Consider the canonical band structure of systems with quenched or static disorder. Localized states exist near the lower band edge. These localized states and the extended states immediately above them are rigorously partitioned at the energy V_0, which is the energy difference between the lowest-lying extended state in the presence and absence of disorder. For our lattice model, the lattice-gas-induced disorder is annealed to fermionic configurations, and an average V_0 can be defined for the ''most probable'' lattice gas distributions. To ensure that extended and localized states do not exist at the same energy, the constraint

$$E_k - \rho_b \bar{v}_0 < V_0 \tag{4}$$

is applied. V_0 is estimated for the appropriate ρ_b in a way that will be described in Sec. IV A, *neglecting the presence of localized fermions*. Localized fermions might be expected to bias the blocker configurations and therefore V_0. When the cavity packing fraction is small, this will not be a serious approximation.

The Gibbs free energy per molecule is

$$\begin{aligned} G(P,\chi_b,T) &= f/(\rho_b+2\rho_e)-P/(\rho_b+2\rho_e)+\mu_b\chi_b+\mu_e\chi_e \\ &= \mu_b\chi_b+\mu_e\chi_e, \end{aligned} \tag{5}$$

where $\chi_b=\rho_b/(\rho_b+2\rho_e)$ and $\chi_e=1-\chi_b$. This expression is to be compared with the Gibbs free energies of other phases to determine the stable thermodynamic phase.

Void size and shape fluctuations are neglected in this treatment. Our approach is reminiscent of theories for cross links in rubber vulcanization.[35] In that case as well, one should consider a distribution of monomer localization lengths to obtain the proper percolation properties.[35] Nevertheless, the assumption of a single, optimal localization length scale already gives reasonable results. Another concern is our neglect of weak localization phenomena,[36] which states that fermions may be localized in an infinite system, but may exhibit no particular length scale. In the absence of blocker–blocker interaction and of long-ranged fermion–blocker attraction, all fermionic states are localized above the percolation threshold of $\rho_{qp}=0.55$,[37] where weak localization dominates. In three dimension, when $\rho_b \leqslant 0.3$ at least, weak localization effects are not significant, and the void description of localized states is valid.[38] ρ_{qp} should shift to higher values in the presence of attractive forces. In this paper, $\rho_b \leqslant 0.5$ in the homogeneous, extended fermion phase, well below the percolation threshold.

C. Extended fermion phase

The infinite U present in Eq. (1) makes straightforward application of mean-field theories difficult. This problem can be circumvented by rewriting the partition function as[39]

$$\begin{aligned} Z &= \mathrm{Tr}_{\{n_i\}}\mathrm{Tr}'_{\{c_i^+c_i\}} \exp(-\beta H), \\ H &= -t\sum_{\langle ij\rangle\sigma}(1-n_i)c_{i\sigma}^+c_{j\sigma}(1-n_j)-\mu_e\sum_{i\sigma}{}' c_{i\sigma}^+c_{i\sigma} \\ &\quad -\mu_b\sum_i n_i-\sum_{ij\sigma}{}' v_{ij}c_{i\sigma}^+c_{i\sigma}n_j, -(1/2)\sum_{ij} w_{ij}n_in_j. \end{aligned} \tag{6}$$

Hopping into blocked-off ($n_i=1$) sites is forbidden in the above Hamiltonian. This strong-coupling formulation captures the physics of the problem succinctly: The energy U does not appear, because fermions never sample the lattice-gas occupied sites, but run around them. The lattice gas is explicitly coupled to the kinetic energy, which leads to a mass renormalization.

The primes on the trace and summation signs denote the constraint that $c_{i\sigma}^{+}c_{i\sigma}=0$ whenever $n_i=1$, and $\mathrm{Tr}'_{\{c_i^{+}c_i\}}$ is dependent on the blocker configurations. The two traces can be made independent by introducing auxiliary fermions at chemical potential $\mu_e(1-\alpha)$ on the blocked-off sites. These fermions do not exhibit hopping, i.e., they are formally lattice gas particles, and their free energy cost, $2\Lambda_i=2\log\{1+\exp[\beta\mu_e(1-\alpha)]\}$ for site i where $n_i=1$, can be exactly subtracted out. With their introduction, Eq. (6) becomes

$$Z=\mathrm{Tr}_{\{n_i\}}\mathrm{Tr}_{\{c_i^{+}c_i\}}\exp[-\beta(H+H_{\mathrm{aux}})], \tag{7}$$

$$H_{\mathrm{aux}}=-t\sum_{\langle ij\rangle\sigma}(1-n_i)c_{i\sigma}^{+}c_{j\sigma}(1-n_j)-\sum_{i\sigma}[\Lambda_i+(1-\alpha)\mu_e]n_ic_{i\sigma}^{+}c_{i\sigma},$$

where fermions occupying $n_i=1$ sites are auxiliary fermions. By introducing the additional degrees of freedom, the constrained summations are thus explicitly removed. This procedure also amounts to applying in reverse the lattice influence functional method often used in classical lattice problems with excluded volume interactions.[40] Counting the auxiliary fermions, there are always $2N$ fermionic and N blocker degrees of freedom. This allows us to introduce a reference Hamiltonian with the same number of degrees of freedom,

$$H_0=-\bar{t}\sum_{\langle ij\rangle\sigma}c_{i\sigma}^{+}c_{j\sigma}-\bar{\mu}_e\sum_{i\sigma}c_{i\sigma}^{+}c_{i\sigma}-\bar{\mu}_b\sum_i n_i, \tag{8}$$

where no distinction has has been made between real and auxiliary fermions. A Gibbs–Bogoliubov–Feynman variational treatment can immediately be applied, giving ($\beta=1$ henceforth)

$$\begin{aligned}\bar{f}&=[-\log Z_0+\langle H+H_{\mathrm{aux}}-H_0\rangle_0]/N\\&=-2\int_k\log(1-\rho_k)-\log(1-\rho_b)-2(\mu_e-\bar{\mu}_e-\alpha\mu_e\rho_b)\bar{\rho}_e-2[(1-\rho_b)^2t-\bar{t}]\langle\epsilon\rangle-(\mu_b-\bar{\mu}_b)\rho_b\\&\quad+2\log[1+e^{\mu_e(1-\alpha)}]\rho_b-2v_0\bar{\rho}_e\rho_b(1-\rho_b)-(1/2)w_0\rho_b^2.\end{aligned} \tag{9}$$

Here $\rho_k=\{1+e^{-(1-\rho_b)^2\Delta_k-\mu_e+\bar{\phi}+(u_0+\alpha\mu_e)\rho_b^2}\}^{-1}$, $\rho_b=1/(1+e^{-\mu_b})$ is the blocker density, $\bar{\rho}_e=\int_k 1/(1+e^{E_k-\bar{\mu}_e})$, $\langle\epsilon\rangle=\int_k E_k/(1+e^{E_k-\bar{\mu}_e})$, $E_k=-2\bar{t}(\cos k_x+\cos k_y+\cos k_z)$, and k are the reciprocal vectors for plane waves. Finally, $v_0=\Sigma_j v_{ij}$ and $w_0=\Sigma_j w_{ij}$.

The value of α is arbitrary, and is optimized along with the three variational parameters in Eq. (8). Setting the first derivatives of $\bar{f}$ to zero, we obtain

$$\bar{\rho}_e=1/[1+e^{-\mu_e(1-\alpha)}], \tag{10}$$

$$\bar{\mu}_b=2(v_0-\alpha\mu_e)\bar{\rho}_e-4(1-\rho_b)t\langle\epsilon\rangle+\mu_b-2\log[1+e^{\mu_e(1-\alpha)}]-4v_0\bar{\rho}_e\rho_b+w_0\rho_b, \tag{11}$$

$$\bar{\mu}_e=\mu_e(1-\alpha\rho_b)+v_0\rho_b(1-\rho_b), \tag{12}$$

$$\bar{t}=(1-\rho_b)^2t. \tag{13}$$

The (single-spin) fermion density is $\rho_e=-(1/2)\partial\bar{f}/\partial\mu_e=(1-\rho_b)\bar{\rho}_e$. Therefore $\rho_b+\rho_e\leqslant 1$, and the exclusion constraint is satisfied on the average. This interesting result only obtains if α is properly optimized as in Eq. (10). Hence, in some nontrivial way, α serves as a density constraint. Note that Eq. (13) exhibits the band-narrowing effect alluded to in Sec. I.

Equation (10) governs the density of the auxiliary fermion. The role of α, which parametrizes the Hamiltonian (*not* the reference Hamiltonian), is unusual and warrants further discussion. The Feynman bound method gives an upper bound on the approximate Helmholtz free energy, Eq. (9), irrespective of α. Optimal α obtains when the original Hamiltonian is identical in structure with the reference Hamiltonian, i.e., when the former has explicitly noninteracting degrees of freedom. The Feynman treatment is exact for such α. In the limit that $t=v_{ij}=0$, or equivalently at infinite temperature, $\alpha=0$ gives this exact result, thus reproducing the important classical limit. For $t>0$, exact results are not known except in special cases. At small ρ_e and low temperature, ρ_e lies at the Fermi level which is large and negative. $\alpha>0$ gives rise to a favorable, attractive on-site coupling $\alpha\mu_e$ between the Fermion and blockers [see Eq. (7)]. However, if $\alpha\geqslant 1$, the logarithmic term in the effective blocker chemical potential becomes large, which would dramatically raise the cost of the lattice gas. The optimal α in Eq. (10) turns out to be of order $1-O(t^{-1})$, or very close to unity. It only slightly affects the effective lattice gas chemical potential, and provides a compromise between the competing demands. α thus interpolates between the exact results at high temperature and a reasonable mean-field description at low temperature. The attractive on-site interaction between fermions and blockers offsets the overestimation of fermion–blocker repulsion present in the hopping term in Eq. (13).

Equations (10)–(13) constitute a classical spin analog of the mean-field slave-boson theory used to treat Hubbard models.[23,24] A finite U formulation of this auxiliary fermion method is also possible.[41] It is found that the present set of equations emerge as the natural large U limit of that theory.

The Gibbs free energy is computed at constant pressure, temperature, and chemical composition. As in Sec. II B, this is achieved by adjusting μ_e and μ_b.

D. Two-phase region

When the repulsive interaction between fermions and blockers dominates, phase separation occurs between a fermion-rich phase (''<'') and a blocker-rich phase (''>''). In the two-phase region, μ_e is identical for both phases, and so is μ_b. For simplicity, the two phases in coexistence are always assumed to involve extended fermionic states and not localized states. Fixing P and T, we trace through $0<\chi_b<1$, solve for Eqs. (10)–(13), and graphically locate the $\chi_b^{<}$ and $\chi_b^{>}$ with matching chemical potentials. The two-phase region is bracketed by these two compositions, i.e., it occurs for $\chi_b^{<}<\chi_b<\chi_b^{>}$. Outside this range, only one phase can exist. The Gibbs free energy per molecule in the two-phase region is given by

$$= \mu_b \chi_b + \mu_e \chi_e , \tag{14}$$

where χ_b and χ_e are as defined above, and the total blocker and Fermion densities are

$$\rho_b = \nu \rho_b^{<} + (1-\nu)\rho_b^{>} ,$$
$$\rho_e = \nu \rho_e^{<} + (1-\nu)\rho_e^{>} . \tag{15}$$

ν is the volume fraction of phase ''<,''

$$\nu = [\rho_b^{>}(1-\chi_b) - 2\rho_e^{>}\chi_b]/[(\rho_b^{>} - \rho_b^{<})(1-\chi_b) + 2(\rho_e^{<} - \rho_e^{>})\chi_b]. \tag{16}$$

For the purposes of estimating the Gibbs free energy of the two-phase region away from the critical point, it is sufficient to assume that the coexisting phases are purely fermions (for ''<'') and purely blockers (''>'') and use the corresponding chemical potentials of the pure systems at the required temperature and pressure. The approximate Gibbs free energy is then

$$G = \nu \mu_b \chi_b + (1-\nu)\mu_e \chi_e , \tag{17}$$

where $\nu = 2\rho_e \chi_b / [\rho_b(1-\chi_b) + 2\rho_e \chi_b]$.

III. FLUCTUATIONS AND STRUCTURE FACTORS

Mean-field theories derived using the Feynman variational method often have one-to-one correspondence with the saddle point approximations to judiciously chosen field theories.[42] By identifying the field theory, loop expansions can be performed and correlation functions derived in a systematic fashion. In this section, scalar fields are used to decouple the fermionic and lattice gas degrees of freedom for the extended fermion phase. The fluctuations will be evaluated to Gaussian (or ''1-loop'') order.

First we introduce the scalar field ϕ_i on each site i, such that

$$Z \propto \int \mathscr{D}\phi \ \mathrm{Tr}_{c_i^+ c_i} \ \mathrm{Tr}_{\{n_i\}} e^{-H - H_{\mathrm{aux}}} \Pi_i \left[\delta\left(\sum_j u_{ij}^{-1} \phi_j + n_i \right) \right]. \tag{18}$$

The Dirac δ functions allow us to remove all $c_i^+ c_i - n_j$ and $n_i - n_j$ couplings by replacing at least one n_i in H with $-\sum_j u_{ij}^{-1}\phi_j$. Then these δ functions are removed via the identity

$$\delta\left(\sum_j u_{ij}^{-1} \phi_j + n_i \right) \propto \int_{-i\infty}^{i\infty} d\sigma_i \exp\left[-\left(\sum_j u_{ij}^{-1}\phi_j + n_i \right)\sigma_i \right]$$

on each site i. Finally the partition function is expanded using the Grassmann algebra path integral formalism,[42,43]

$$Z[\lambda, \xi] \propto \int \mathscr{D}\phi \int \mathscr{D}\sigma \int \mathscr{D}(\bar{\psi}\psi) \mathrm{Tr}_{\{n_i\}} e^{-S},$$
$$S = \sum_{ij} \phi_i u_{ij}^{-1} \sigma_j + (1/2) \sum_{ijkl} \phi_i u_{ij}^{-1} w_{jk} u_{kl}^{-1} \phi_l - t \sum_{\langle ij \rangle \sigma} \int_\tau \left(1 + \sum_k u_{ik}^{-1}\phi_k \right) \bar{\psi}_{i\sigma\tau} \psi_{j\sigma\tau} \left(1 + \sum_l u_{jl}^{-1}\phi_l \right)$$
$$+ \sum_{ij\sigma} \int_\tau \phi_i \bar{\psi}_{i\sigma\tau} \psi_{i\sigma\tau} u_{ij}^{-1} \phi_j + \alpha\mu_e \sum_{ikl\sigma} \int_\tau u_{ik}^{-1}\phi_k \bar{\psi}_{i\sigma\tau}\psi_{i\sigma\tau} u_{il}^{-1}\phi_l - \sum_{i\sigma} \int_\tau \bar{\psi}_{i\sigma\tau}(\mu_e - \partial/\partial\tau - \phi_i - \lambda_i)\psi_{i\sigma\tau}$$
$$+ \sum_{ijk} \phi_i u_{ij}^{-1} w_{jk} n_k - \sum_i \int_\tau \{\mu_b - 2\log[1 + e^{\mu_e(1-\alpha) - \lambda_i}] - \sigma_i - \xi_i\} n_i , \tag{19}$$

where $\bar{\psi}_{i\sigma\tau}, \psi_{i\sigma\tau}$ are the Grassmann fields on site i, spin σ, and Euclidean time index τ, and λ_i and ξ_i are generating fields introduced to evaluate structure factors. The Grassmann variables anticommute, $\psi_1\psi_2 + \psi_2\psi_1 = 0$, and vanish when taken to any integral power higher than one, $\psi_1^n = 0$, $n > 1$.

The Grassmann fields and lattice gas degrees of freedom are completely decoupled in Eq. (19), and standard loop expansions can be readily applied. The σ_i scalar fields are purely imaginary in this formulation. However, for the purpose of evaluating the saddle point and the fluctuations via the steepest descent method, they are rotated on to the real axis. So σ_i will henceforth be treated as real variables. The Hubbard–Stratonovich transform presented above can generalized using complex Gaussian fields.[41] It is also worth noting that the ϕ field couples to the change in spin-summed fermion density, or the charge density fluctuations. Spin density fluctuations exist, but, in the absence of fermion–fermion interaction and external magnetic field, do not couple to other degrees of freedom. The two fields ϕ and σ together govern the fluctuations in the concentration gradient as well as in the total particle density.

The mean field theory of Sec. II C is readily rederived as the saddle point approximation to Eq. (19). On taking derivatives with respect to ϕ_i and σ_i, and assuming translational invariance, $\phi_i = \bar{\phi}$ and $\sigma_i = \bar{\sigma}$, one finds that ($u_0 = v_0 - \alpha\mu_e$)

$$\bar{\phi} = -u_0 \rho_b , \tag{20}$$

$$\bar{\sigma} = -2u_0 \bar{\rho_e} + 4(1-\rho_b) t\langle \epsilon \rangle + 4v_0 \bar{\rho_e} \rho_b . \tag{21}$$

Equating the coefficients in Eqs. (19) and (8), it is found that

$$\overline{\mu}_b \leftrightarrow \mu_b - \overline{\sigma} - 2\log[1+e^{\mu_e(1-\alpha)}] + w_0\rho_b, \tag{22}$$

$$\overline{\mu}_e \leftrightarrow \mu_e - \overline{\phi} - \overline{\phi}^2\left(\sum_j u_{ij}^{-1} + \alpha\mu_e \sum_{jl} u_{ij}^{-1}u_{il}^{-1}\right) = \mu_e + \mu_0\rho_b(1-\rho_b) - \alpha\mu_e\rho_b^2. \tag{23}$$

Equations (20)–(23) coincide with Eqs. (11)–(13). Hence the mean-field equations of Sec. II C are recovered.

By applying standard one-loop expansions[42,43] on the fields ϕ_i and σ_i in Eq. (19), one obtains the corrections to the free energy

$$\begin{aligned}\delta \log Z \approx & -(1/2)\int_k \log(-\hat{u}_k^2 \det M_k) + (1/2)\rho_b(1-\rho_b)\int_k |\hat{\xi}_k - 2\overline{\rho}_e\hat{\lambda}_k|^2 - (1/2) \\ & \times \int_k \begin{bmatrix} M_k^{\phi\lambda}\hat{\lambda}_k + M_k^{\phi\xi}\hat{\xi}_k \\ \rho_b(1-\rho_b)(\hat{\xi}_k - 2\overline{\rho}_e\hat{\lambda}_k)\end{bmatrix} M_k^{-1} \begin{bmatrix} M_k^{\phi\lambda}\hat{\lambda}_{-k} + M_k^{\phi\xi}\hat{\xi}_{-k} \\ \rho_b(1-\rho_b)(\hat{\xi}_{-k} - 2\overline{\rho}_e\hat{\lambda}_{-k})\end{bmatrix} \\ & - \rho_b\overline{\rho}_e(1-\overline{\rho}_e)\int_k |\lambda_k|^2 + (1-\rho_b)^{-2}\int_{k_1,k_2} \frac{\rho_{k_1}-\rho_{k_2}}{\Delta_{k_1}-\Delta_{k_2}}\,\delta_{k-k_1+k_2}|\hat{\lambda}_k|^2,\end{aligned} \tag{24}$$

where

$$M_k^{\sigma\sigma} = \rho_b(1-\rho_b), \tag{25}$$

$$M_k^{\phi\sigma} = -\hat{u}_k^{-1} + \rho_b(1-\rho_b)\hat{u}_k^{-1}\hat{w}_k, \tag{26}$$

$$\begin{aligned}M_k^{\phi\phi} = & 2(1-\rho_b)^{-2}\int_{k_1,k_2} \frac{\rho_{k_1}-\rho_{k_2}}{\Delta_{k_1}-\Delta_{k_2}}\{-(1-\rho_b) \\ & + \rho_b\hat{u}_k^{-1}(v_0+\alpha\mu_e) + (1-\rho_b)\hat{u}_k^{-1}[\Delta_{k_1}+\Delta_{k_2}]\}^2 \\ & \times \delta_{k-k_1+k_2} - \hat{u}_k^{-2}\hat{w}_k + \rho_b(1-\rho_b)\hat{u}_k^{-2}\hat{w}_k^2 \\ & + 4\int_{k_1,k_2} \rho_{k_1}\Delta_{k_2}\hat{u}_k^{-2}\delta_{k-k_1+k_2} - 4\int_{k_1} \rho_{k-k_1}\hat{v}_k\hat{u}_k^{-2},\end{aligned} \tag{27}$$

$$\begin{aligned}M_k^{\lambda\lambda} = & 2(1-\rho_b)^{-2}\int_{k_1,k_2} \frac{\rho_{k_1}-\rho_{k_2}}{\Delta_{k_1}-\Delta_{k_2}}\,\delta_{k-k_1+k_2} \\ & - 2\rho_b\overline{\rho}_e(1-\overline{\rho}_e),\end{aligned} \tag{28}$$

$$\begin{aligned}M_k^{\phi\lambda} = & 2(1-\rho_b)^{-2}\int_{k_1,k_2} \frac{\rho_{k_1}-\rho_{k_2}}{\Delta_{k_1}-\Delta_{k_2}}\,\delta_{k-k_1+k_2}\{(1-\rho_b) \\ & - \hat{u}_k^{-1}[\rho_b(u_0+\alpha\mu_e) + (1-\rho_b)(\Delta_{k_1}+\Delta_{k_2})]\}\end{aligned} \tag{29}$$

$$- 2\rho_b(1-\rho_b)\overline{\rho}_e\hat{u}_k^{-1}\hat{w}_k, \tag{30}$$

$$M_k^{\phi\xi} = \rho_b(1-\rho_b)\hat{u}_k^{-1}\hat{w}_k. \tag{31}$$

The 2×2 Hessian matrix, $-M_k$,

$$M_k = \begin{pmatrix} M_k^{\phi\phi} & M_k^{\phi\sigma} \\ M_k^{\sigma\phi} & M_k^{\sigma\sigma}\end{pmatrix}, \tag{32}$$

governs the fluctuations in $\hat{\phi}_k$ and $\hat{\sigma}_k$ and determines the stability of the system. Setting the generating fields $\hat{\lambda}_k = \hat{\xi}_k = 0$, the correction to the pressure becomes

$$\beta\delta P = -(1/2)\int_k \log(-\hat{u}_k^2 \det M_k). \tag{33}$$

Equations (24)–(33) are the main results of this section.

Since the Gibbs ensemble is used in this work, Eq. (33) should in principle be added to Eq. (9) to evaluate the pressure. ρ_b and ρ_e are also renormalized by the fluctuations.[44] In this work, the Gaussian corrections are only used to assess the validity of the saddle point solution, to locate the onset of instability, and in particular, to generate the structure factors.

The fermion–fermion, fermion–blocker, and blocker–blocker correlation functions obtains from the functional derivatives with respect to the generating fields,

$$C_{bb}(ij) = \langle n_i n_j\rangle = \frac{\partial^2}{\partial\xi_i\partial\xi_j}\log Z,$$

$$C_{eb}(ij) = \langle c_{i\sigma}^+ c_{i\sigma} n_j\rangle = \frac{\partial^2}{\partial\lambda_i\partial\xi_j}\log Z, \tag{34}$$

$$C_{ee}(ij) = \int_\tau \langle c_{i\sigma\tau}^+ c_{i\sigma\tau} c_{j\sigma}^+ c_{j\sigma}\rangle = \frac{\partial^2}{\partial\lambda_i\partial\lambda_j}\log Z.$$

In the last line, $c_{i\sigma\tau}^+ = \exp\{+\tau H_0\}c_{i\sigma}^+\exp\{-\tau H_0\}$. To mean-field order, blockers are uncorrelated with fermions, while the fermion–fermion structure factors are those for free fermions. To Gaussian order, one carries out the functional differentiations in Eq. (34) with respect to Eq. (24). The results are

$$\hat{C}_{bb}(k)=D^{-1}(k)[\rho_b(1-\rho_b)]^2M_k^{\phi\phi}\hat{u}_k^2+\rho_b(1-\rho_b)+D^{-1}(k)[\rho_b(1-\rho_b)]^2\hat{w}_k[2-\rho_b(1-\rho_b)\hat{w}_k], \tag{35}$$

$$\hat{C}_{eb}(k)=-2\overline{\rho_e}\rho_b(1-\rho_b)+D^{-1}(k)\rho_b(1-\rho_b)\hat{u}_kM_k^{\phi\lambda}-2D^{-1}(k)[\rho_b(1-\rho_b)]^2\overline{\rho_e}M_k^{\phi\phi}\hat{u}_k^2-2D^{-1}(k)\times\overline{\rho_e}\rho_b^2(1-\rho_b)^2\hat{w}_k[1-\rho_b(1-\rho_b)\hat{w}_k], \tag{36}$$

$$\hat{C}_{ee}(k)=2(1-\rho_b)^2\int_{k_1,k_2}\frac{\rho_{k_1}-\rho_{k_2}}{\Delta_{k_1}-\Delta_{k_2}}\,\delta_{k-k_1+k_2}+D^{-1}(k)\rho_b(1-\rho_b)(\hat{u}_kM_k^{\phi\lambda})^2-4\overline{\rho_e}\rho_b(1-\rho_b)\hat{u}_kM_k^{\phi\lambda}[1-\rho_b(1-\rho_b)\hat{w}_k]+4D^{-1}(k)[\rho_b(1-\rho_b)\overline{\rho_e}]^2M_k^{\phi\phi}\hat{u}_k^2-2\rho_b\overline{\rho_e}(1-\overline{\rho_e})+4\rho_b(1-\rho_b)\overline{\rho_e}^2, \tag{37}$$

where

$$D(k)=-\hat{u}_k^2\det M_k=[1-\rho_b(1-\rho_b)\hat{w}_k]^2-\rho_b(1-\rho_b)\hat{u}_k^2M_k^{\phi\phi}. \tag{38}$$

The $\overline{\rho_e}$ terms arise from the auxiliary fermions. In the parameter space of interest here, $\overline{\rho_e}$ is generally small, and the terms that contain $\overline{\rho_e}$ are typically small too.

In the absence of auxiliary fermions and the exclusion constraints, the expressions derived in this section reduce to the ''random phase approximation'' for a two-component system with fermion–lattice gas interaction $\hat{u}_k$. When $\rho_e\to 0$, the fluctuations and structure factors of an Ising model with w_{ij} interactions obtain to Gaussian order.

The mean-field calculation is performed on a spherical Fourier space grid. The agreement between the spherical grid approximation and a full cubic grid calculation is generally excellent. This is because the fermion coverage is small, of order of a few percent at the most. Only the low-lying k states, which can be effectively described without reference to the lattice structure, are strongly occupied at reasonably low temperatures. In fact, the most significant part of the phase diagram is close to $\chi_b\sim 1$, where the fermion density is the lowest. The fluctuations and structure factors are also computed using a spherical grid. The constant square well potentials defined on the 3-d lattice are approximated by spherical step functions with appropriately chosen radii. It is found that the positions and heights of the major peaks in the structure factors are in good agreement with the results of full calculations performed using a cubic grid.

IV. RESULTS

A. $\rho_e\to 0$: The quantum percolation limit

In the $\rho_e\to 0$ limit, the blockers do not respond to the presence of delocalized fermions. In the case of noninteracting blockers ($w_{ij}=0$) and purely excluded volume interaction ($v_{ij}=0$), the physics of the quantum percolation problem[37] should be recovered. In our mean-field theory, the small ρ_e limit amounts to taking $T=0$ and setting $\overline{\mu_e}$ at the bottom of the extended fermionic band. The optimal α is 1^-. Equations (12) and (13) lead to

$$\overline{\mu_e}=-6(1-\rho_b)^2t,\qquad \mu_e=\overline{\mu_e}/(1-\rho_b). \tag{39}$$

As a result, $\mu_e=-6t+6\rho_bt$. This means that V_0, the shift in the lowest conduction state energy from the $\rho_b=0$ value, is equal to $6\rho_bt$. By comparison, the exact V_0 obtained via the transfer matrix method[37] and by path integral simulation[38] is approximately $4\rho_bt$ at small ρ_b. So Eq. (39) gives a reasonable estimate of the percolation threshold, and in the small ρ_e regime, the mean-field theory should be a reasonable starting point. Incidentally, the infinite dimension exact result predicts the scaling $t\to(1-\rho_b)t$ at infinite U,[14] and it also gives $V_0=6\rho_bt$ when the hopping matrix element is properly scaled with the dimensionality.

When a long-ranged attractive interaction is present, the mean-field mobility edge is

$$V_0=6\rho_bt-v_0\rho_b. \tag{40}$$

It is this V_0 that will be applied in constraining the energy levels of the cavities in Eq. (2). Since $v_0=\Sigma_j v_{ij}>\overline{v_0}$ [see Eq. (3)], Eqs. (4) and (40) suggest that no levels are allowed in the cavity phase when the attractive interaction is extremely large. Indeed, localized electrons are never found in

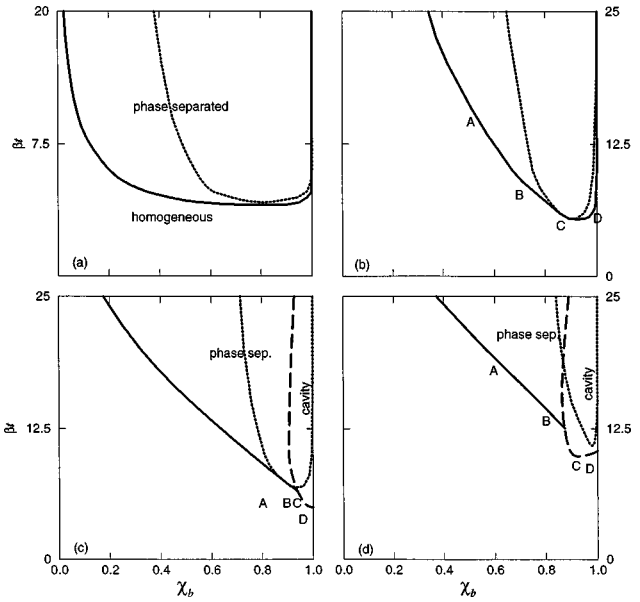

FIG. 2. Mean-field phase diagrams. (a) $\beta P=0.6$, $\epsilon=0$, $\omega=0$; (b) $\beta P=0.6$, $\epsilon=0.1$, $b=1$, $\omega=0$; (c) $\beta P=0.65$, $\epsilon=0.16$, $b=1$, $\omega=0.002$, $d=2$; (d) $\beta P=0.4$, $\epsilon=0.175$, $b=1$, $\omega=0.002$, $d=2$. The dotted lines indicate the onset of instability. For (b), (c), and (d), divergences first occur at finite k along the low χ_b branches of the spinodal lines. The dashed lines describe the boundaries of the cavity phase.

fluids like argon, where the interaction with excess electrons is predominantly attractive.[45] In this work, only moderate attractive interactions are considered.

B. Phase diagram: Exclusion forces

The mean-field phase diagram for purely excluded volume interaction ($v_{ij}=0$, $w_{ij}=0$) is shown in Fig. 2(a), where $\beta P=0.6$. At high temperature, the thermal de Broglie wavelength is small and fermions are not highly degenerate. The system is a mixture of two types of similar lattice gases, and a homogeneous phase obtains. The fermion states in the two-phase region have energies $\sim V_0$ below those for the homogeneous phase. At low temperature, the favorable energy of demixing dominates the entropy of mixing, and phase segregation occurs. The coexistence curve is highly asymmetric, especially when the critical point occurs at low temperature. ρ_e is generally small, of order 0.1%–2% for $\beta t \geqslant 5$, even at high χ_e (low χ_b). This is because a degenerate Fermi gas can exert enormous pressure even at low density. In contrast, the pressure exerted by the blockers is athermal, and $\rho_b=0.451$ for the neat blocker phases irrespective of temperature. ρ_b in Fig. 2(a) is well below the quantum percolation threshold.[37]

The dotted lines mark the onset of instability in the mean-field solution of Sec. II C. Along those lines, $D(k)$ vanishes at $k=0$ and the fluctuations diverge [Eq. (38)]. The critical point of phase coexistence and the turning point of the instability line are very close but do not coincide. This is an artifact caused by the introduction of auxiliary fermions. The structure factors exhibit Ising-like behavior, peaking at $k=0$, as will be described in detail in Sec. IV D.

No cavity phase is found in the absence of attractive interactions. A representative histogram of the Gibbs free energy $G(a)$ computed at discrete cavity sizes $a=V_a^{1/3}$ is shown in Fig. 3(a). It is seen that larger cavities are progressively more favorable, and $G(a)$ asymptotes to the phase coexistence value given by Eq. (17). Our conclusion is that phase separation is always more favorable than cavity formation. The fermion occupancies are also shown in Fig. 3(a). Small cavities accommodate one fermion of each spin. Larger cavities contain more fermions, and the optimal case is $a\to\infty$, in which case the occupation number is macroscopic.

These findings are somewhat different from the work of Alavi and Frenkel,[22] which predicts a proliferation of voids. It seems that their cavities actually mimic the homogeneous extended fermion phase. Furthermore, they do not apply the $E_k<V_0$ constraint, and this allows small cavities that support localized states isoenergetic with conduction states. Even if that constraint were lifted, however, small voids are still found to be unstable with respect to phase separation in our treatment. The contrasting predictions stem from the different treatments of multiple occupancy. Alavi and Frenkel allow only one electron per cavity. The argument for single electron voids dates back to Lifshitz[46] and runs as follows. An isolated fermion in an extended state costs roughly $\beta f_e \sim \beta\rho_b t$. At low temperature, it is more favorable for the fermion to reside in a cavity devoid of offending molecules. The free energy of the resulting localized fermion consists of

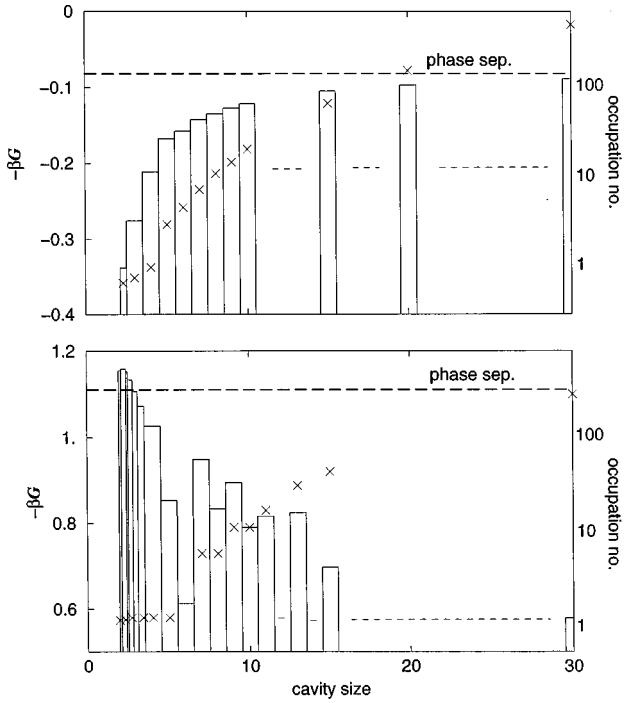

FIG. 3. Gibbs free energy of the cavity phase vs cavity size at $\chi_b=0.99$. (a) $\beta P=0.3$, $\beta t=20$, $\epsilon=0$, $\omega=0$; (b) $\beta P=0.4$, $\beta t=11$, $\epsilon=0.175$, $b=1$, $\omega=0.002$, $d=2$. The dashed line indicates the Gibbs free energy of the two phase region. ''x'' gives the occupation number per spin per cavity.

the entropic cost of creating the cavity plus the kinetic energy of confinement, i.e., $\beta f_l \sim \rho_b a^3 + 3\beta t\pi^2/a^2$. a is the void size, and the second term is the particle-in-a-cubic-box kinetic energy. Optimizing with respect to a, it is found that $f_l<f_e$ at sufficiently low temperature. In Fig. 2(a), the cavity state is stable when $\beta t \geqslant 32.5$, which corresponds to a thermal de Broglie wavelength of 5.7. Under these conditions, $\beta f_l \approx 88$, and so cavities are extremely costly.

When a macroscopic number of fermions are present, and provided that the medium can respond to the fermion configurations, multiply occupied cavities are more favorable than single ones. Consider two fermions in a cubic box, one each in the ground and first excited state. By the particle-in-a-box estimate, the total kinetic energy is now $9t\pi^2/a^2$. Optimizing, it is found that a doubly occupied void is more favorable than two single ones. The situation for spherical cavities is similar, and cavity shape fluctuations renders double occupancy even more favorable. Finally, as the occupancy increases, the cavities grow larger, the electronic states become lower in energy, and high occupancies become progressively more favorable. The result of this nucleationlike chain of events is phase separation. Our conclusion is that phase separation pre-empts any possible cavity phase. The mechanism stated above is consistent with phase separation of the normal, energy-driven, domain-growth mediated variety. Indeed (to use the anology of Ref. 9 again), if fermions and blockers simply repel each other just like like oil and water, then it is physically reasonable that they phase separate at low temperature rather than form microemulsion like cavity structures. Cavity states have been observed in irradiated helium fluids, which are basically hard, spherical

TABLE I. Factors that favor the formation of the different phases, to mean-field order.

	Extended fermion phase	Cavity phase	Phase segregation	Modulated phase
βt	Small	Intermediate	Large	Large
βP or ρ_b	Small (at reasonably small ϵ)	Large	Large	Finite
ϵ	Finite	Intermediate	0	Large
b	Indifferent	Large	0	Large
ω	0	Large	Large	0

blockers.[47] The unscreened Coulomb repulsion between electrons stabilizes the singly occupied cavities in that system. However, the maximum cavity concentration in fluid helium is only of order $\sim 10^8$ cm^{-3},[48] which translates into $\chi_e \sim 10^{-14}$.

C. Phase diagram: Attractive fermion–lattice gas interaction

Next the effect of attraction between fermions and blockers is investigated. Consider a simple square well potential,

$$v_{ij} = \epsilon, \quad i \neq j, \quad |i-j|_{x,y,z} \leq b. \tag{41}$$

The lattice gas–lattice gas interaction is also modeled as a square well,

$$w_{ij} = \omega, \quad i \neq j, \quad |i-j|_{x,y,z} \leq d. \tag{42}$$

The roles played by these two interactions are as follows. As ϵ increases from zero, competing forces between the on-site exclusion and the longer-ranged attraction develop. It is favorable for the fermions to be far away from blockers for kinetic energy reasons, but an attractive interaction is gained when they are close together. A compromise is reached when fermions reside in cavities devoid of blockers. In the cavity regime, fermions and blockers attract each other through their contact at the void boundary, i.e., it is a surface term. As the cavity size increases, the surface-to-volume ratio decreases and stabilization is not as effective. At phase separation, or when $a \to \infty$, the fermion–blocker attraction vanishes in the thermodynamic limit. Hence $\epsilon > 0$ stabilizes the cavity phase with respect to phase separation.[49]

However, $\epsilon > 0$ also favors modulated phases for very similar reasons. It is also energetically favorable for blockers to be arranged in periodic arrays, leaving relatively unconstricted channels in which the fermions can negotiate and interact favorably with the blockers in their vicinity. Incommensurate modulated phases also occur in finite-U Kimball–Falicov models.[18] Metal ammonia solutions phase segregate at low temperature; they do not form periodic, solidlike structures. A better description of these systems obtains if we also include lattice gas–lattice gas attraction. This provides a thermal driving force for the lattice gas to aggregate, and in particular enhances the stability of the two-phase region at zero temperature over that of periodic phases.

To illustrate these points, Fig. 2(b) shows the phase diagram for $\beta P = 0.6$ with $\epsilon = 0.1$, $b = 1$, and $\omega = 0$. There are 26 sites within the range of v_{ij}. Compared with Fig. 2(a), also computed at $\beta P = 0.6$, the attractive interaction partially cancels the on-site repulsion and renders the homogeneous phase more favorable. The low χ_b branch of the instability line marks the points where $D(k)$ first vanishes at *finite* k. Around the critical point, and along the high χ_b branch of the instability line, fluctuations first diverge at $k = 0$.

$\epsilon = 0.1$ is not large enough to stabilize the cavity phase with respect to other phases. A cavity phase emerges at $\epsilon = 0.14$. However, at such large attractions, the finite k instabilities pre-empt the low χ_b branch of the coexistence curve *and* the critical point. This is the signature of incommensurate modulated phases. To eliminate these modulated phases, $\omega = 0.002$ and $d = 2$ are applied in Figs. 2(c) and 2(d). βP and ϵ are (0.65, 0.16) and (0.4, 0.175), respectively. Under these conditions, a narrow strip of the cavity phase appears over a range of temperatures. The optimal cavity size a is shown in Fig. 3(b). The smallest cavities are the most stable, and $G(a)$ exhibits nonmonotonic progression at large a due to lattice effects.[50] At high temperature, extended states are more readily populated, and the delocalized fermion phase is favored over the cavity phase. At very low temperature, the system relaxes to its most energetically favorable configurations, and phase separation takes place. This explains the fact that the cavity phase tapers off at both ends of the temperature axis [Figs. 2(c) and 2(d)].

The above discussions suggest that many competing factors contribute to the stability of the various phases. These considerations are summarized in Table I.

The metal–insulator transition is identified as the phase boundary between the cavity phase and the extended fermion phase. These two phases are in reality not separate thermodynamic entities, but are limiting extrapolations of the same homogeneous phase containing both localized and extended electrons. The ''transition'' should really be a crossover, but it is sufficiently sharp at room temperature that such a description is warranted.[1] For a qualitative comparison, Deng *et al.*[9] find that electrons are localized at $\chi_e \sim 0.02$, and bicontinous percolating channels exist when $\chi_e \sim 0.09$. The metal–insulator transition occurs somewhere in between; experimentally, it is known to take place at $\chi_e \sim 0.04$–0.05. In Figs. 2(c) and 2(d), the transition happens at $\chi_e < 0.07$ and $\chi_e \sim 0.14$, respectively, and depends on the temperature and the parameters used. These estimates are of the same order magnitude as the simulation results. It is cautioned that the cavity packing fraction can reach almost 30% at $\chi_e \sim 0.14$ in this work. At such coverage, neither the estimates for V_0 nor the independent cavity approximation are quantitative.

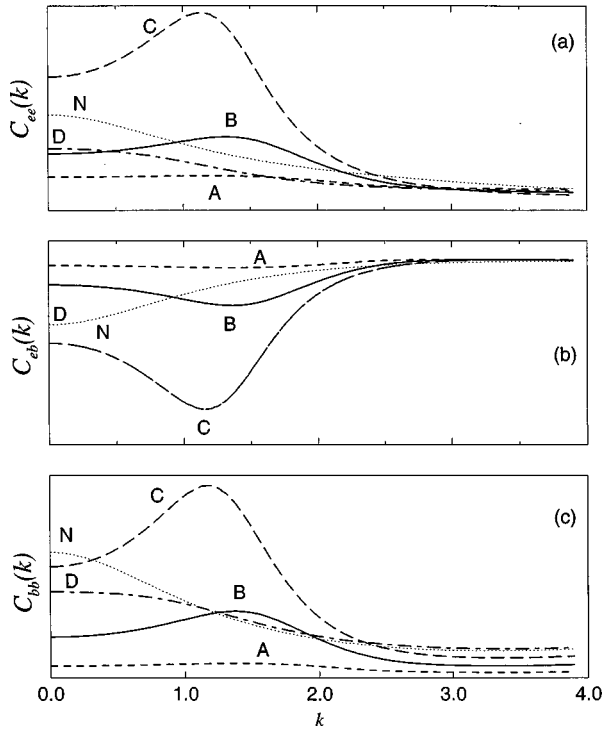

FIG. 4. Structure factors at the points indicated in Fig. 2(b) ($\beta P=0.6$, $\epsilon=0.1$, $\omega=0$). (a) $\hat{C}_{ee}(k)$; (b) $\hat{C}_{eb}(k)$; (c) $\hat{C}_{bb}(k)$. The dotted lines (labeled ''N'') are sample structure factors for the phase diagram in Fig. 2(a), where only exclusion interaction exists between fermions and blockers.

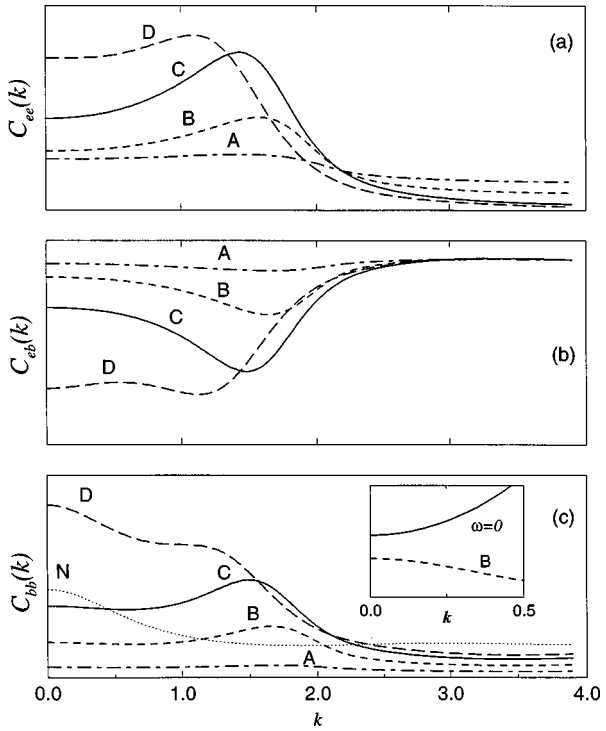

FIG. 5. Structure factors at the points indicated in Fig. 2(d) ($\beta P=0.4$, $\epsilon=0.175$, $b=1$, $\omega=0.002d$, $d=2$). The symbols are as in Fig. 4. The dotted line in panel (c), labeled ''N,'' depicts $\hat{C}_{bb}(k)$ for the pure blocker (i.e., Ising) system at the same temperature and pressure. Inset: comparison between the small-k behavior at point B in Fig. 2(d) and a representative point in Fig. 2(b), in which $\omega=0$.

D. Structure factors

Figures 4 and 5 plots the structure factors at points $A-D$ along the coexistence curves in Figs. 2(b) and 2(d), respectively. $\hat{C}_{ee}(k)$, $\hat{C}_{bb}(k)$, and $\hat{C}_{eb}(k)$ all exhibit structures at $k_c=1-1.8$ at sufficiently large χ_e in Figs. 4 and 5, which take into account both the on-site exclusion interaction and the longer-ranged attraction. They indicate the formation of structures at characteristic length scales of 3–6 lattice sites. As the fermion concentration decreases and the critical point is approached, the peak in the structure factors shifts to smaller k, signaling an increase in the characteristic length scale. By contrast, the system in Fig. 2(a) only includes exclusion forces, and the interplay between the competing forces is absent. The corresponding structure factors (dotted lines in Fig. 4) are Ising-like, peaking at $k=0$ at all χ_e.

The phase diagram in Fig. 2(c) gives a metal–insulator transition closest to the experiment values of $\chi_e\sim 0.04$. In Fig. 6, our structure factors computed on an isotherm are compared to scattering experiments and to the all-atom structure factor computed at $\chi_e=1-\chi_b=0.09$ in Ref. 9. The simulation structure factor peaks at $(k\sigma_{\mathrm{NH}_3})_c=1.4$ [Fig. 1(c)], where σ_{NH_3} is the ammonia Lennard-Jones diameter. This peak arises from the bicontinuity, and characterizes the mean separation between the percolating channels.[9] Our structure factors, derived by assuming that the fermions percolate through space, therefore strongly suggest that the present model exhibits bicontinuity, with percolating channels 3–6 lattice sites apart. k_c decreases with decreasing χ_e and eventually vanishes for $\chi_e>0$ [see point D in Figs. 2(b) and 4]. The positions of ''superstructure'' peaks or shoulders observed in Li– and Na–NH_3 small angle x-ray scattering[51] and small angle neutron scattering[52] experiments also shift towards $(k\sigma_{\mathrm{NH}_3})_c=0$ as χ_e decreases. Our results and Ref. 9 suggest that these previously unexplained trends are due to the increasing separation of percolating channels. The electrical conductivity should be sensitive to such structural changes.[53] The theoretical k_c [experimental Li–NH_3 $(k\sigma_{\mathrm{NH}_3})_c$] values are 0.95 (1.3), 1.55 (2.1), and 1.70 (3.1) at $\chi_e=0.044$, 0.10, and 0.16, respectively. Quantitative comparison for $\chi_e<0.04$ is hampered by the small shoulders predicted by the theory. While experiments, theory, and simulations are in reasonable agreement for $\chi_e\leqslant 0.1$, the lattice model does not model the fluid accurately at small length scales. $(k\sigma_{\mathrm{NH}_3})_c$ is sensitive to the identity of the cation.[51] The functional form of v_{ij} can be varied to model this dependency.

The $\hat{C}_{bb}(k)$ in Figs. 5 and 6 and experimental structure factors[51] all contain $k=0$ components. In our model, these features reflect $w_{ij}>0$, and are absent for structure factors in system with no blocker–blocker interactions ($\omega=0$) [Fig. 4; inset of Fig. 5(c)], whose intermediate k behavior are otherwise similar.

To analyze the peak position, which is relatively temperature independent, consider low temperature and small ρ_e. First let $\omega=0$, whereupon $\hat{C}_{bb}(k)$ (modulo a constant) is entirely due to the fermions, and its small k behavior determines k_c. Furthermore, $M_k^{\phi\xi}=0$ and $M_k^{\phi\sigma}=\hat{u}_k^{-1}$. From Eqs. (25) to (27) and Eq. (34), we have

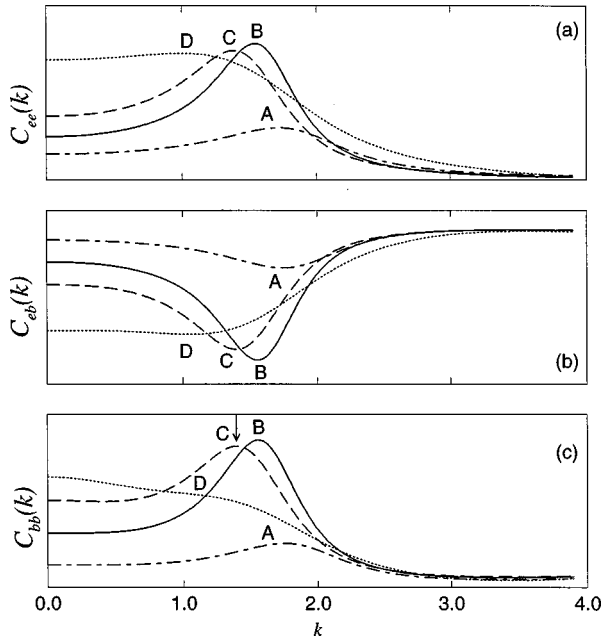

FIG. 6. Structure factors at the points indicated in Fig. 2(c) ($\beta P=0.65$, $\epsilon=0.16$, $b=1$, $\omega=0.002$, $d=2$). The y axes have been scaled and shifted. The arrows indicate the peak position at 9% Li molar fraction ($\chi_b=0.91$) computed in Ref. 9.

$$\hat{C}_{bb}(k)\propto\frac{1}{(\mathscr{M}_k)^{-1}-1}\sim\frac{1}{M_0+M_2k^2+O(k^4)}, \tag{43}$$

where $\mathscr{M}_k$ is $\rho_b(1-\rho_b)M_k^{\phi\phi}\hat{u}_k^2$, $M_0=\mathscr{M}_0^{-1}-1>0$ due to mechanical stability, $M_2=-(1/2\mathscr{M}_0^2)\partial^2\mathscr{M}_k/\partial k^2|_{k=0}$ $\propto(k_F^{-2}-c\epsilon)$, $k_F=(6\pi^2\rho_e)^{1/3}$, and the positive scalar c is ρ_e independent. At large k_F and ϵ, $M_2<0$. From Eq. (43), this means that $k_c>0$ and $\hat{C}_{bb}(k)$ [Fig. 4(c)] exhibit the characteristic form of microemulsionlike structure factors.[54] In microemulsions, the surface tension is small, which favors segregation of the pure species on mesoscopic/microscopic length scales and leads to bicontinuity.[33] In our model, as ρ_e decreases, k_F decreases, M_2 eventually changes sign, and k_c vanishes. This analysis shows that the superstructure in $\hat{C}_{bb}(k)$ arises from the competition between the fermion kinetic energy (the k_F^{-2} term) and the fermion–blocker attraction, i.e., it has the same origin as the cavity states. Furthermore, it is a purely quantal effect, absent for $t\to 0$.

At $\omega=0.002$ and $\epsilon=0.16$ [Fig. 2(c)], the phases of metal ammonia solutions are reproduced. At this ω, M_2 is always positive, and $\hat{C}_{bb}(k)$ has a $k=0$ peak over the entire χ_b range, in agreement with experiments. The $\hat{C}_{bb}(k)$'s are therefore not microemulsionlike for small k. However, at length scales of 3–6 lattice sites, the superstructures persist, and the physics that governs microemulsions applies.

It is also profitable to compare with other systems that exhibit bicontinuous phases. In oil–water–surfactant mixtures, the emergence of the finite k peak marks the onset of the microemulsion phase, and the characteristic length scales decrease as the surfactant concentration increases.[55] Higher surfactant concentrations give rise to more frustration in the system. In our model, the magnitude of ϵ is a rough measure of the competition between attraction and repulsion. ϵ is larger in Fig. 6 than in Fig. 4, and indeed the characteristic structures are generally of shorter lengthscales in the former case.

V. DISCUSSION

There are differences between the lattice model proposed in this work and real metal ammonia solutions. (a) The phase diagrams shown in Figs. 2(c) and 2(d) are supercritical with respect to the lattice gas, whose mean-field critical point lies at $(\beta t)_c=16$ and $(\rho_b)_c=0.5$, far away from the phase boundaries of interest. Liquid ammonia is subcritical at temperatures at which experiments on metal ammonia solutions are conducted. Supercritical conditions are used because the liquid (high density) branch of the lattice gas coexistence curve occurs at $\rho_b\sim 1$, which is undesirable for modeling liquid ammonia. Among other things, most electronic states would be localized at such blocker densities. (b) Because lattice models limit the energy and entropy of cavity formation and favor the formation of modulated structures, cavities are found close to the critical point. In metal ammonia solutions, cavities dominate over a larger range of temperature.

In spite of these limitations, the present work appears to capture four main features of metal ammonia solutions: (a) the existence of a cavity-dominated regime; (b) the existence of an extended fermion phase which shows bicontinuous behavior; (c) phase segregation at low temperature; and (d) a metal–insulator transition at the boundary between the cavity phase and the homogeneous phase. It is hoped that these findings will lead to more detailed theoretical treatments of fermion–fluid mixtures.

Since two different theories are applied to the two homogeneous phases, it is impossible to satisfy phase coexistence between the extended Fermion phase and the cavity phase. Future extension of this work should therefore unify the extended and localized states treatments. Electron–electron interactions should also in incorporated to reproduce the fine details of the localized phase. At low electron concentration ($\chi_e\leqslant 0.02$), our prediction is that the main peaks in the structure factors shift to $k=0$. In x-ray scattering experiments, superstructures with finite characteristic length scales persist at and below such electron concentrations. It is likely these structures arise from the correlation between cavities[56] neglected in this work.

Finally, we stress that the fermion–blocker repulsion dominates the attractive force in our work, giving rise to fermion–blocker demixing at low temperature. The cavity phase then arises from the surface energy terms. In contrast to previous predictions, cavities are found to be unstable toward phase separation in the absence of the attractive interaction between Fermions and fluid. In the opposite limit, i.e., where attraction dominates, the localized states are expected to from around droplets of high density fluctuations in the fluid at low electron concentrations.[11,57] These localized states may be unstable to phase separation of a different type at high electron concentration. Here, because of the strong attraction, phase separation should occur between a regime with high densities of *both* blockers and Fermions, and a regime with low densities of both components.

ACKNOWLEDGMENTS

This work was completed in the Department of Chemistry at U.C. Berkeley. One of us (K.L.) is indebted to Professor K. B. Whaley for her generosity and support. We would also like to thank Hyung-June Woo, Carlo Carraro, Richard Stratt, Robert A. Harris, and Mike L. Klein, for their useful comments, and David Chandler for suggesting a lattice model treatment of metal ammonia solutions.

[1] J. C. Thompson, *Electrons in Liquid Ammonia* (Oxford University Press, London, 1976).
[2] *Physics and Chemistry of Electrons and Ions in Condensed Matter*, edited by J. Acrivos (Reidel, New York, 1984).
[3] *Metal-Ammonia Solutions*, edited by G. Lepoutre and M. J. Sienko (Benjamin, New York, 1963).
[4] *Electrons in Fluids*, edited by J. Jortner and N. R. Kestner (Springer, Berlin, 1973).
[5] Proceedings of Colloque Weyl V, J. Phys. Chem. **84**, 1065 (1980); Colloque Weyl VI, *ibid.* **88**, 3699 (1984); Colloque Weyl VII, J. Phys. IV **1**, (1991).
[6] Z. Phys. Chem. (Neue Folge) **184**, pt. 1-2 (1994).
[7] P. Chieux *et al.*, J. Phys. IV **1**, 3 (1991), and references therein.
[8] The existence of electrons localized in cavity states has also been verified in computer simulations. See, for example, M. Marchi, M. Sprik, and M. L. Klein, J. Phys.: Condens. Matter **2**, 5833 (1990); Z.-H. Deng, G. J. Martyna, and M. L. Klein, Phys. Rev. Lett. **68**, 2496 (1992); G. J. Martyna, Z.-H. Deng, and M. L. Klein, J. Chem. Phys. **98**, 555 (1993).
[9] Z.-H. Deng, M. L. Klein, and G. J. Martyna, J. Chem. Soc., Faraday Trans. **90**, 2009 (1994); Z.-H. Deng, G. J. Martyna, and M. L. Klein, J. Chem. Phys. **100**, 7590 (1994); Phys. Rev. Lett. **71**, 267 (1993).
[10] R. M. Stratt, Annu. Rev. Phys. Chem. **40**, 61 (1990).
[11] D. Chandler and K. Leung, Annu. Rev. Phys. Chem. **45**, 557 (1994).
[12] L. M. Falicov and J. C. Kimball, Phys. Rev. Lett. **22**, 997 (1969).
[13] M. Plischke, Phys. Rev. Lett. **28**, 361 (1972).
[14] U. Brandt and C. Mielsch, Z. Phys. B **75**, 365 (1989); **79**, 295 (1990); **82**, 37 (1991).
[15] J. L. Lebowitz and N. Macris, J. Stat. Phys. **76**, 91 (1994); T. Kennedy, Rev. Math. Phys. **6**, 901 (1994); J. L. Lebowitz and N. Macris, *ibid.* **6**, 927 (1994); A. Messager and S. Miracle-Sole, *ibid.* **8**, 271 (1996).
[16] Q.-M. Si, G. Kotliar, and A. Georges, Phys. Rev. B **46**, 1261 (1992).
[17] P. Farkasovsky, Phys. Rev. B **52**, R5463 (1995), and references therein.
[18] J. K. Freericks, Phys. Rev. B **47**, 9263 (1993).
[19] A. Schiller and K. Ingersent, Phys. Rev. Lett. **75**, 113 (1995).
[20] F. Wegner, Z. Phys. B **35**, 207 (1979).
[21] A. J. McKane and M. Stone, Ann. Phys. (N.Y.) **131**, 36 (1981).
[22] A. Alavi and D. Frenkel, J. Chem. Phys. **97**, 9249 (1992).
[23] S. E. Barnes, J. Phys. F **6**, 1375 (1976); **7**, 2637 (1977).
[24] G. Kotliar and A. E. Ruckenstein, Phys. Rev. Lett. **57**, 1362 (1986).
[25] M. Kahlweit *et al.*, J. Colloid Interface Sci. **118**, 436 (1987).
[26] G. Gompper and M. Schick, *Self-Assembling Amphiphilic Systems* (Academic, San Diego, 1994).
[27] The resemblance between the two systems has been often pointed out by Professor D. Chandler, for example, during the STATPHYS 19 Conference, China, 1995 (unpublished).
[28] F. Hensel and H. Uchtmann, Annu. Rev. Phys. Chem. **40**, 61 (1989).
[29] The electron–electron repulsion leads to the formation of peanut-shaped bipolarons, where the singlet electrons are localized in two cavities in close contact (Ref. 9). Neglecting the fermion–fermion interaction results in fermions of opposite spins localized in the same cavity (this work). However, no significant spatial correlations *between* bipolarons are observed (Ref. 9). Hence the effect of the Coulomb interaction seems to be short-ranged in the cavity-dominated regime.
[30] M. Sprik, J. Phys. IV **1**, 99 (1991).
[31] T. C. Kavanaugh and R. M. Stratt, J. Chem. Phys. **100**, 3028 (1994).
[32] T. Koslowski, D. G. Rowan, and D. E. Logan, Int. J. Phys. Chem. **100**, 101 (1996); D. E. Logan, I. J. Bush, and P. A. Madden, Z. Phys. B (Neue Folge) **184**, 25 (1994).
[33] The various mesophases in oil–water–surfactant mixtures have also been captured by a lattice model with only short-ranged, mutually frustrating forces. See K. A. Dawson, M. D. Lipkin, and B. Widom, J. Chem. Phys. **88**, 5149 (1988); B. Widom, *ibid.* **84**, 6954 (1986).
[34] K. Leung and F. S. Csajka, Phys. Rev. Lett. **78**, 3721 (1997).
[35] A. Zippelius, P. M. Goldbart, and N. Goldenfeld, Europhys. Lett. **23**, 451 (1993); P. M. Goldbart and A. Zippelius, Phys. Rev. Lett. **71**, 2256 (1993); H. E. Castillo, P. Goldbart, and A. Zippelius, Europhys. Lett. **28**, 519 (1994).
[36] E. Abrahams, P. W. Anderson, D. C. Licciardello, and T. V. Ramakrishnan, Phys. Rev. Lett. **42**, 673 (1979).
[37] C. M. Soukoulis, Q.-M. Li, and G. S. Grest, Phys. Rev. B **45**, 7724 (1992).
[38] K. Leung and D. Chandler, J. Chem. Phys. **102**, 1405 (1995).
[39] C. J. Thompson, T. Matsubara, and Y. S. Yang, Prog. Theor. Phys. **91**, 251 (1994).
[40] See, for example, D. Frenkel and A. A. Louis, Phys. Rev. Lett. **68**, 3363 (1992).
[41] K. Leung (unpublished).
[42] J. W. Negele and H. Orland, *Quantum Many-Particle Systems* (Addison–Wesley, Redwood City, 1988).
[43] D. Belitz and T. R. Kirkpatrick, Rev. Mod. Phys. **66**, 261 (1994).
[44] G. Parisi, *Statistical Field Theory* (Addison–Wesley, Redwood City, 1988), Chap. 10.
[45] R. A. Holroyd and W. F. Schmidt, Annu. Rev. Phys. Chem. **40**, 439 (1989).
[46] I. M. Lifshitz, Usp. Fiz. Nauk **83**, 617 (1964) [Sov. Phys. JETP **7**, 549 (1965)].
[47] C. C. Grimes and G. Adams, Phys. Rev. B **45**, 2305 (1992); **41**, 6366 (1990).
[48] J. P. Hernandez, Rev. Mod. Phys. **63**, 675 (1991).
[49] See also C. Carraro, Physica A **236**, 130 (1997), on the role of long-ranged attractions in the formation of cavities.
[50] $G(a)$ for the cavity phase does not approach its phase coexistence value even for large a [Fig. 3(b)] because of the $E_k<V_0$ constraint. The correct $a\rightarrow\infty$ limit *is* recovered if the constraint is lifted. It seems that the cavity mean field theory is a poor starting point for recovering phase segregation when ϵ is large.
[51] D. N. Knapp and H. D. Bale, J. Appl. Crystallogr. **11**, 606 (1978).
[52] P. Chieux and H. Bertagnolli, J. Phys. Chem. **88**, 3726 (1984).
[53] J. Jortner and M. H. Cohen, J. Chem. Phys. **58**, 5170 (1973).
[54] In typical microemulsions, $M_2<0$; see M. Teubner and R. Strey, J. Chem. Phys. **87**, 3195 (1987).
[55] H.-J. Woo, C. Carraro, and D. Chandler, Phys. Rev. E **52**, 6497 (1995).
[56] M. L. Klein (private communications).
[57] J. P. Hernandez, J. Phys. C **16**, 3465 (1983).